

Rational Design of Thermoresponsive Microgel Templates with Polydopamine Surface Coating for Microtissue Applications

Elena Stengelin, Brice Nzigou Mombo, Mihail Mondeshki, Guillermo L. Beltramo, Martin A. Lange, Patrick Schmidt, Hajo Frerichs, Seraphine V. Wegner, and Sebastian Seiffert*

Functional microgels provide a versatile basis for synthetic in vitro platforms as alternatives to animal experiments. The tuning of the physical, chemical, and biological properties of synthetic microgels can be achieved by blending suitable polymers and formulating them such to reflect the heterogenous and complex nature of biological tissues. Based on this premise, this paper introduces the development of volume-switchable core-shell microgels as 3D templates to enable cell growth for microtissue applications, using a systematic approach to tune the microgel properties based on a deep conceptual and practical understanding. Microscopic microgel design, such as the tailoring of the microgel size and spherical shape, is achieved by droplet-based microfluidics, while on a nanoscopic scale, a thermoresponsive polymer basis, poly(*N*-isopropylacrylamide) (PNIPAAm), is used to provide the microgel volume switchability. Since PNIPAAm has only limited cell-growth promoting properties, the cell adhesion on the microgel is further improved by surface modification with polydopamine, which only slightly affects the microgel properties, thereby simplifying the system. To further tune the microgel thermoresponsiveness, different amounts of *N*-hydroxyethylacrylamide are incorporated into the PNIPAAm network. In a final step, cell growth on the microgel surface is investigated, both at a single microgel platform and in spheroidal cell structures.


1. Introduction

Microtissue engineering is a significant development in the field of 3D cell culture technology, as the design of microtissue platforms reflects the diversity and complexity of in vivo environments, thereby providing excellent alternatives to animal testing. As animal experiments face ethical and moral concerns, they are increasingly blocked by law and need to be reduced, replaced, and refined according to the 3R concept by Russel and Burch from 1959.^[1] Classical 2D cell cultures may appear to be such a substitute, but they only inadequately reflect the complex in vivo conditions.^[2,3] To overcome that limitation, the development of 3D cell culture in vitro models is needed, especially such models that mimic the hierarchical structure of in vivo environments in a simplifying manner.

In this context, an increasing amount of research deals with the fabrication of microtissue-based spheroidal 3D in vitro models using scaffold-free and scaffold-assisted methods. While the scaffold-free

E. Stengelin, M. Mondeshki, M. A. Lange, P. Schmidt, H. Frerichs, S. Seiffert
Department of Chemistry
Johannes Gutenberg-University Mainz
Mainz D-55128, Germany
E-mail: sebastian.seiffert@uni-mainz.de

B. Nzigou Mombo, S. V. Wegner
Institute of Physiological Chemistry and Pathobiochemistry
Westfälische Wilhelms-University Münster
Münster D-48149, Germany
G. L. Beltramo
Institute of Biological Information Processing 2 (IBI-2)
Forschungszentrum Jülich GmbH
Jülich D-52428, Germany

 The ORCID identification number(s) for the author(s) of this article can be found under <https://doi.org/10.1002/mabi.202100209>

© 2021 The Authors. Macromolecular Bioscience published by Wiley-VCH GmbH. This is an open access article under the terms of the Creative Commons Attribution License, which permits use, distribution and reproduction in any medium, provided the original work is properly cited.

DOI: 10.1002/mabi.202100209

method does not require any matrix at all, the scaffold-promoted method uses additional hydrogel-based matrix elements to form cell spheroids. For this purpose, several research studies are especially focused on the encapsulation of cells in poly(ethylene glycol) (PEG)-based microgels. In these microgels, cells preferentially interact with other cells, forming cell spheroids due to the antifouling property of PEG.^[4,5] Compared to 2D cell culture models, these cell spheroids effectively mimic a 3D environment by growing in a network-like structure instead of growing on a flat substrate. However, these cells also grow without control in all three dimensions, ignoring the intrinsically defined and hierarchically structured *in vivo* environment. In view of the general motivation of replacing animal experiments by synthetic platforms, a better-defined basis of 3D *in vitro* models is therefore necessary, which additionally takes into account the shape, the nature, and the mechanical properties of *in vivo* tissues to best mimic the *in vivo* environment. To address this issue and to contribute to that basis, we aim at a rational design of microgel-based templates with functional and at the same time cell-adhesive properties for the engineering of complex microtissue constructs.

An appropriate material for our intent is the stimuli-responsive poly(*N*-isopropylacrylamide) (PNIPAAm). Hydrogels made from this polymer exhibit a reversible volume phase transition (VPT) in the physiological temperature range and undergo changes in solubility and swelling, which facilitates the imitation of the structure, properties, and microenvironment of native tissue.^[6–8] By incorporation of comonomers into the PNIPAAm network, the VPT temperature can be further tuned to higher or lower values depending on the hydrophilicity and the amount of the comonomer.^[9] Since PNIPAAm-based microgels can be easily shaped via droplet-based microfluidics, various temperature-dependent microgels can be obtained, which differ in size, mechanical strength, and opacity.^[10] As a result, this approach enables the rational material design of specific and tuneable microgel-based microcarrier cores and provides a good platform for precisely directed microtissue templating.

The other key point for the successful implementation of the microgel templates is to increase their cell affinity. In general, PNIPAAm hydrogels show a temperature-dependent cell affinity, such that above the VPT temperature, cells show increased cell adhesion and proliferation on PNIPAAm-coated culture dishes, whereas when the temperature is decreased, the cells are detached from the culture dish.^[11] Hence, to make the templates more versatile, temperature-independent cell adhesion on the PNIPAAm microgels needs to be supported. To address this objective, we use a polydopamine (PDA) coating, which is a cost-effective and biocompatible solution providing potentially high cell affinity and maintaining the microgels' VPT properties.^[12] Moreover, PDA adheres to a variety of surfaces with strong binding forces, as Messersmith's group has demonstrated.^[13,14] In a preliminary work to our study, Zhang et al. have adapted this method for producing PDA-coated PNIPAAm-based nanogels.^[15] The approach translates well to PNIPAAm-based microgels, thus enabling the synthesis of highly cell-affine and multifunctional core-shell microcarriers.

Based on this strategy, this work presents the manufacturing of well-designed core-shell microgels, which are suitable templates

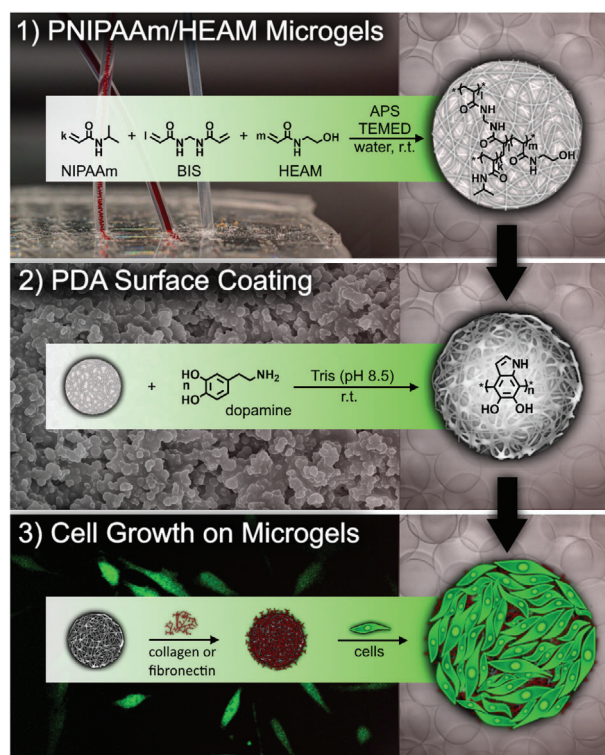


Figure 1. PDA-coated PNIPAAm/HEAM-based core-shell microgels as templates for microtissue applications in three steps: 1) PNIPAAm/HEAM microgel (core) synthesis by droplet-based microfluidics. The microgel network is based on NIPAAm, BIS crosslinker and different amounts of HEAM comonomer, which react in a radical polymerization to form stable networks initiated by TEMED and APS. 2) PDA surface modification of PNIPAAm/HEAM-based microgels (shell) to increase the microgels' cell adhesiveness. 3) Cell coating experiments of PNIPAAm/HEAM-PDA microgels improved by previous collagen or fibronectin coating of the microgels.

for fine-structured microtissues mainly due to their dual functionality (VPT properties of the core and cell growth-promoting properties of the shell). Our approach involves three steps, as shown in **Figure 1**: The first step 1) focuses on the microgel design and synthesis, the second step 2) on the PDA surface coating of the microgels to increase their cell adhesion properties, and the third step 3) on the cell growth experiments on microgels. For this purpose, we use a systematic parameter control and enable targeted tuning of the microgel properties at multiple levels. On a nanoscopic scale, we choose temperature-sensitive and cell-affine materials, while on a microscopic level, the templating of the PNIPAAm-based microgels is performed by droplet-based microfluidics and subsequent PDA-surface coating. At the same time, the microgel core properties, such as their size and mechanical strength, are controlled at the mesoscopic level by additional incorporation of the hydrophilic comonomer *N*-hydroxyethylacrylamide (HEAM). Based on this systematic approach, our platform offers a great variety of well-designed PNIPAAm/HEAM core-shell microgel templates and provides a promising basis for complex and advanced 3D *in vitro* cell culture systems with deep understanding on a conceptual and practical level as alternative for animal testing.

Table 1. Composition of the 0, 2.5, 7.5, and 12.5 mol% PNIPAAm/HEAM polymer networks. The amounts of PNIPAAm, HEAM, and BIS in the respective systems are indicated as x in mol%. Proton ratios (proton ratio_{NMR}) of PNIPAAm (H-c) and HEAM (H-f, H-e) comonomers are calculated as $\text{proton ratio}_{\text{NMR}} = (A_{\text{PNIPAAm}}/A_{\text{HEAM}})^{-1} 4H$, using the proton integrals of PNIPAAm (A_{PNIPAAm}) and HEAM (A_{HEAM}), experimentally determined by ^1H MAS NMR spectroscopy (Figure S1 and Table S1, Supporting Information). For comparison, the molar ratios of PNIPAAm (n_{PNIPAAm}) and HEAM (n_{HEAM}) comonomers are calculated as molar ratio = $(n_{\text{PNIPAAm}}/n_{\text{HEAM}})^{-1}$ (Table S2, Supporting Information).

	x PNIPAAm [mol%]	x HEAM [mol%]	x BIS [mol%]	Proton ratio _{NMR}	Molar ratio
0 mol%	99.0	0.0	1	—	—
2.5 mol%	96.5	2.5	1	30.41	40.00
7.5 mol%	91.5	7.5	1	13.09	13.33
12.5 mol%	86.5	12.5	1	8.18	8.00

2. Results and Discussion

2.1. PNIPAAm/HEAM Microgels

2.1.1. Polymer Basis

PNIPAAm is chosen to provide a suitable polymer basis for our work due to its thermoresponsiveness in water, by which PNIPAAm hydrogels exhibit temperature-dependent mechanical properties that can be further tuned by incorporating comonomers. Moreover, due to their hydrophilic nature, PNIPAAm-based materials mimic the extracellular matrix well and provide a stable environment as a basis for potential 3D microtissue engineering. Hence, we focus on the development of PNIPAAm-based 3D templates that are designed at several levels. On a nanoscopic level, hydrogels are prepared using NIPAAm monomers and N,N' -methylenebisacrylamide (BIS) as a crosslinker. Dissolved in water and initiated by ammonium persulfate (APS) and N,N,N',N' -tetramethylethylenediamine (TEMED), these molecules react with each other in a radical polymerization and crosslink to form stable gels at room temperature.^[16] Moreover, by incorporating HEAM as a comonomer into the PNIPAAm network, the mechanical properties of the PNIPAAm system can be altered. To analyze the influence of the comonomer on the thermoresponsive PNIPAAm properties, we investigate three different hydrogel systems that differ in the amount of HEAM. Specifically, 2.5, 7.5, and 12.5 mol% of HEAM content are considered, while the NIPAAm content is adjusted accordingly, and the BIS content remains constant at 1 mol%.

2.1.2. Comonomer Content in PNIPAAm/HEAM-Based Hydrogels

To understand and analyze the HEAM influence on our thermoresponsive hydrogel properties, it is necessary to determine the actual comonomer content in the PNIPAAm networks. For this purpose, we investigate the HEAM content in the 2.5, 7.5, and 12.5 mol% PNIPAAm/HEAM polymer networks as well as the HEAM-free PNIPAAm network (0 mol%) swollen in D_2O using quantitative ^1H magic angle spinning NMR spectroscopy (^1H MAS NMR). In the case of gels (as well as semisolid matrixes), the anisotropic interactions like dipole–dipole couplings, quadrupole couplings, and anisotropy of the chemical shift are partially averaged due to the limited mobility of molecules induced by the solvent in the gel. To further reduce the line-broadening, and there-

with to improve the resolution, only low spinning speeds of a few kilohertz are needed. At these conditions, the recorded ^1H MAS NMR spectra mimic those obtained in solution and provide comparable resolution. The investigated polymer compositions are listed in Table 1, while the full ^1H MAS NMR spectra are shown in Figure 2.

There we assign the signal at 3.90 ppm to the methine proton of the isopropyl side group of PNIPAAm (H-c). The peaks at 3.67 and 3.34 ppm are related to the hydroxyethyl side group of HEAM (H-f, H-e). The two resonances at 2.30–1.83 and 1.83–1.32 ppm refer to the backbone protons of the polymer network (H-b, H-a), and those at 1.32–0.90 ppm to the six methyl protons of the PNIPAAm side chain (H-d).^[17] Due to the small amount of BIS (1 mol%) in the polymer network, the related signals are not considered.

The quantification of the HEAM content in the PNIPAAm/HEAM networks is performed based on the H-c, H-f, and H-e proton signals, which are shown enlarged in Figure 2. In this representation, all spectra are referenced to the H-c proton of the PNIPAAm isopropyl side group. Accordingly, from the 2.5 mol% system (gray), over the 7.5 mol% system (red) up to the 12.5 mol% system (green), an increasing intensity of the H-f and H-e proton signals is observed due to the increasing amount of HEAM comonomer within the three copolymer systems. In accordance, no H-f and H-e signals are detected for the 0 mol% (black) system.

Whether the HEAM comonomer incorporation into the PNIPAAm network is stoichiometric can be assessed by determining the integral ratio (proton ratio_{NMR}) between the H-c proton signal (A_{PNIPAAm}) and the H-f and H-e proton signals (A_{HEAM}) of each copolymer system using the formula: $\text{proton ratio}_{\text{NMR}} = (A_{\text{PNIPAAm}}/A_{\text{HEAM}})^{-1} 4H$ (Table 1). Respective A_{PNIPAAm} and A_{HEAM} values are obtained by deconvoluting the ^1H MAS NMR spectra as shown in Figure S1 and Table S1 in the Supporting Information. For comparison, the theoretical molar ratios of NIPAAm (n_{PNIPAAm}) and HEAM (n_{HEAM}) (molar ratio = $(n_{\text{PNIPAAm}}/n_{\text{HEAM}})^{-1}$) are also analyzed (Table S2, Supporting Information) and presented in Table 1. The values of the 12.5 mol% (proton ratio_{NMR}: 8.18, molar ratio: 8.00) and 7.5 mol% (proton ratio_{NMR}: 13.09, molar ratio: 13.33) systems agree well. But deviations are observed in the 2.5 mol% system (proton ratio_{NMR}: 30.41, molar ratio: 40.00), probably due to the small amount of HEAM comonomer used. The lower the amount of comonomer, the more error-prone are the measurements.

In conclusion, HEAM can be assumed to be stoichiometrically incorporated into the PNIPAAm/HEAM networks, as

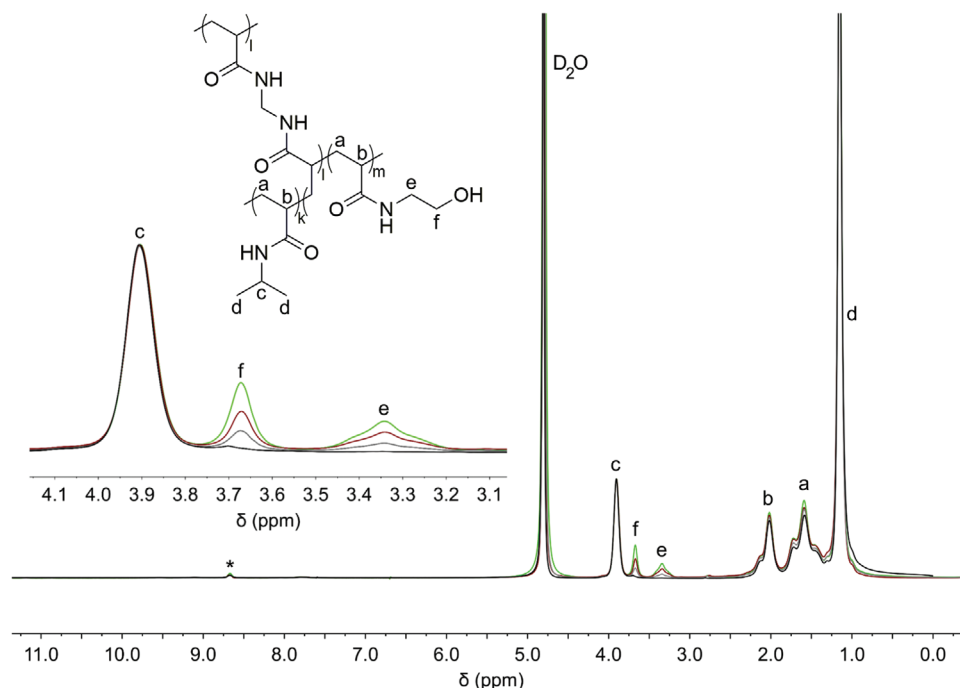


Figure 2. Full ^1H MAS NMR spectra of the 0 mol% (black), 2.5 mol% (gray), 7.5 mol% (red), and 12.5 mol% (green) PNIPAAm/HEAM hydrogels and schematic structure of the polymer network with the proton species assigned. Enlarged sections of the ^1H MAS NMR spectra show relevant signals for the quantification of the HEAM content in the hydrogels at 3.90 (H-c), 3.67 (H-f), and 3.34 ppm (H-e).

the experimentally determined proton ratios_{NMR} agree well with the theoretically calculated values. This finding provides a fundament to classify our subsequent investigations.

2.1.3. Microgel Synthesis via Droplet-Based Microfluidics

To make the 2.5, 7.5, and 12.5 mol% PNIPAAm/HEAM polymer systems useful for microtissue templating, they need to be shaped on a microscopic level. A suitable method to convert the polymer networks into spherical microgels is droplet-based microfluidic templating, which we use for the microgel synthesis. For this purpose, a poly(dimethylsiloxane) (PDMS)-based microchannel device, fabricated by hard and soft lithography, is used as described in Figure S2 in the Supporting Information. The microfluidic channel has a rectangular cross-section of 100 μm in diameter in which the aqueous solution based on NIPAAm, HEAM, BIS, and APS is broken into monodisperse droplets by flow-focusing by an immiscible carrier fluid of fluorinated oil (Novec 7500), surfactant (Krytox), and initiator (TEMED). Stabilized by the oil-surfactant mixture, the NIPAAm, HEAM, and BIS molecules in these droplets react in a free-radical crosslinking polymerization reaction initiated by TEMED that diffuses from the surrounding oil phase into the aqueous droplet within a few minutes, thereby gelling the drops. By breaking the resulting microgel suspension using 1*H*,1*H*,2*H*,2*H*-perfluoro-1-octanol, PNIPAAm/HEAM microgels of type 2.5, 7.5, and 12.5 mol% with diameters between 160 and 180 μm in water are obtained to which the following investigations refer. The size of the microgels can also be adjusted by varying the flow rates of the injected

fluids or by varying the microfluidic channel system width, as described in Figure S3 in the Supporting Information.

2.1.4. Temperature-Dependent Swelling Measurement

To provide a platform of well-designed microgel templates with stimuli-responsive properties, we investigate the three PNIPAAm/HEAM polymer networks and analyze the impact of the HEAM-comonomer on their temperature-dependent swelling. A characteristic quantity of thermoresponsive gels is the volume phase transition temperature (VPTT). At this temperature, the nanoscopic network-strand structure is rearranged due to changing polymer-solvent interactions, thereby causing a change of the microgel volume and elastic properties.

To study temperature as well as solvent influences on the VPTT, PNIPAAm/HEAM microgels are immersed in three different solvents. In detail, the microgels are placed in water as a standard solution and in phosphate buffer as well as Dulbecco's Modified Eagle Medium (DMEM) with 10% fetal bovine serum (FBS), 1% GlutaMAX (Gl.), and 1% penicillin-streptomycin (P/S), which are relevant media for applications in cell biology. While the microgels are immersed in these different solvents, the temperature is increased from 25 to 50 $^{\circ}\text{C}$ at a rate of 0.1 $^{\circ}\text{C min}^{-1}$. At each step, images of the microgels are taken by light microscopy, and their diameters are determined using an image processing program. By plotting the microgel diameters as a function of temperature, temperature-dependent swelling curves are obtained. Such swelling curves of the microgels in water are represented in Figure 3a, while swelling curves of the same microgels in phosphate buffer and DMEM (10% FBS, 1%

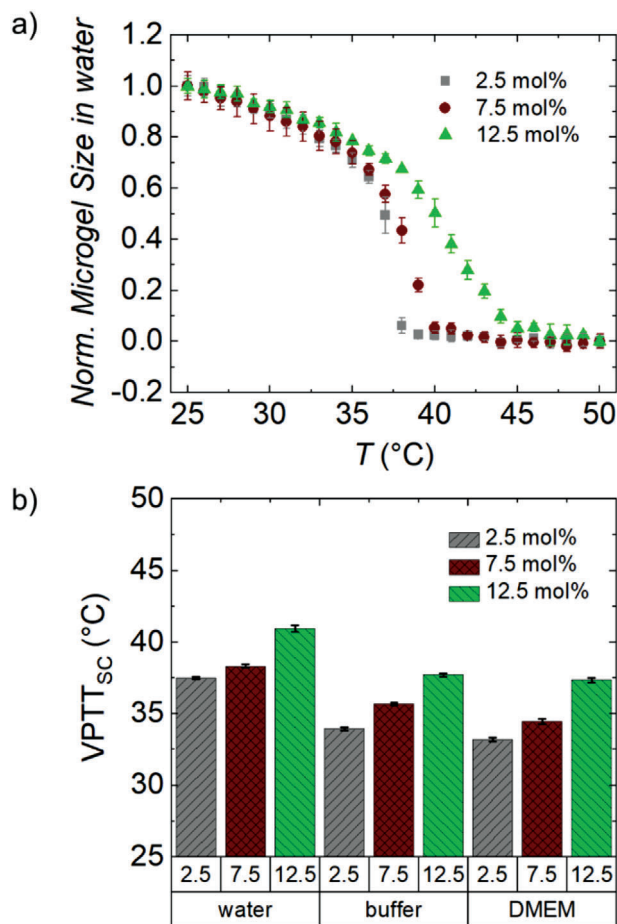


Figure 3. Temperature-dependent swelling of 2.5 mol% (■), 7.5 mol% (●), and 12.5 mol% (▲) microgels. a) Swelling curves in water. b) VPTT_{sc} in water, phosphate buffer, and DMEM (10% FBS, 1% Gl., and 1% P/S).

Gl., and 1% P/S) are shown in Figure S4 in the Supporting Information. The symbols in gray (■) refer to the 2.5 mol%, in red (●) to the 7.5 mol%, and in green (▲) to the 12.5 mol% microgels. When comparing the three swelling curves of microgels in water, two observations can be identified: First, the curves shift toward higher temperatures with increasing comonomer content in the microgel polymer networks from 2.5 mol%, over 7.5 mol% up to 12.5 mol%. Second, the gradients of the respective swelling curves decrease with increasing temperature.

The shift of the swelling curves toward higher temperatures with increasing HEAM comonomer content is explainable by the more hydrophilic character of HEAM compared to that of PNIPAAm.^[9] With increasing HEAM comonomer content, the PNIPAAm/HEAM networks therefore become more hydrophilic, whereby solvents can be better retained in the network at higher temperatures.

The decrease of the swelling-curve gradients of the PNIPAAm/HEAM networks is also explainable by the increasing network hydrophilicity with increasing HEAM content. The more HEAM comonomer is in the network, the less cooperative chain segments collapse in it, resulting in a more widespread VPT.^[9] This trend is well known in literature for

PNIPAAm microgels copolymerized to neutral or charged hydrophilic comonomers.^[18]

From the inflection points of the swelling curves, we further determine the VPTT as a characteristic parameter. The inflection points are calculated by derivation of the swelling curves and subsequent Gaussian fitting, while the maximum of the fit curves corresponds to the inflection points. Derivations and Gaussian fittings of the swelling curves in DMEM (10% FBS, 1% Gl., and 1% P/S) are shown in Figure S5 in the Supporting Information, while the estimated VPTT_{sc} quantities of all three systems in water, phosphate buffer, and DMEM (10% FBS, 1% Gl., and 1% P/S) are represented in Figure 3b and in Table S3 in the Supporting Information.

By comparing the VPTT_{sc} values, it is noticeable that they shift to higher temperature with increasing HEAM comonomer content in all three solvents. The increasing VPTT_{sc} within the three systems is explainable by the same reasons as discussed above. The more hydrophilic HEAM comonomer is incorporated in the PNIPAAm/HEAM polymer networks, the more do the swelling curves and the VPTT_{sc} shift to higher temperatures.

Additionally, the solvent type has a significant influence on the VPTT_{sc}. Compared to the swelling measurements in water, the swelling curves in phosphate buffer and DMEM (10% FBS, 1% Gl., and 1% P/S) shift to lower temperatures. Since phosphate buffer and DMEM (10% FBS, 1% Gl., and 1% P/S) include inorganic salts, this finding is explainable with the competition for solvent molecules between the microgels and salt ions due to the osmotic pressure. This competition effectively strengthens hydrophobic interactions within the polymer network and thereby promotes a VPTT_{sc} at lower temperatures.^[18] Minor differences can also be observed between the VPTT_{sc} of microgels in phosphate buffer and DMEM (10% FBS, 1% Gl., and 1% P/S), but they are small compared to the values in water. These differences may be due to the multitude of ingredients in the DMEM (10% FBS, 1% Gl., and 1% P/S), which all have an influence on the osmotic pressure and hence on the VPTT_{sc} of the polymer networks.

2.1.5. Hydrogel Elasticity

To achieve a general understanding of the polymer-network elasticity on a mesoscopic level, we focus on the mechanical hydrogel properties and examine temperature and solvent influences. These examinations are performed by temperature-dependent rheology measurements in water, phosphate buffer, and DMEM (10% FBS, 1% Gl., and 1% P/S). Respective data are represented in Figure 4, where the storage modulus G' is plotted against the temperature from 25 to 50 °C. Figure 4a displays measurements of the 2.5 mol% (■), 7.5 mol% (●), and 12.5 mol% (▲) hydrogels in plain water as the swelling medium. In all these three systems, G' increases with increasing temperature, which is due to their VPT behavior: with increasing temperature, the polymer systems collapse and expel the solvent. Thus, the hydrogels become smaller, but the amount of polymer in them remains the same, resulting in a higher concentration of the remaining polymer backbone contributing to the deformation resistance, which is why G' increases with increasing temperature.^[19]

Since the three hydrogel systems differ in comonomer content and hence in the VPTT, the G' versus temperature curves

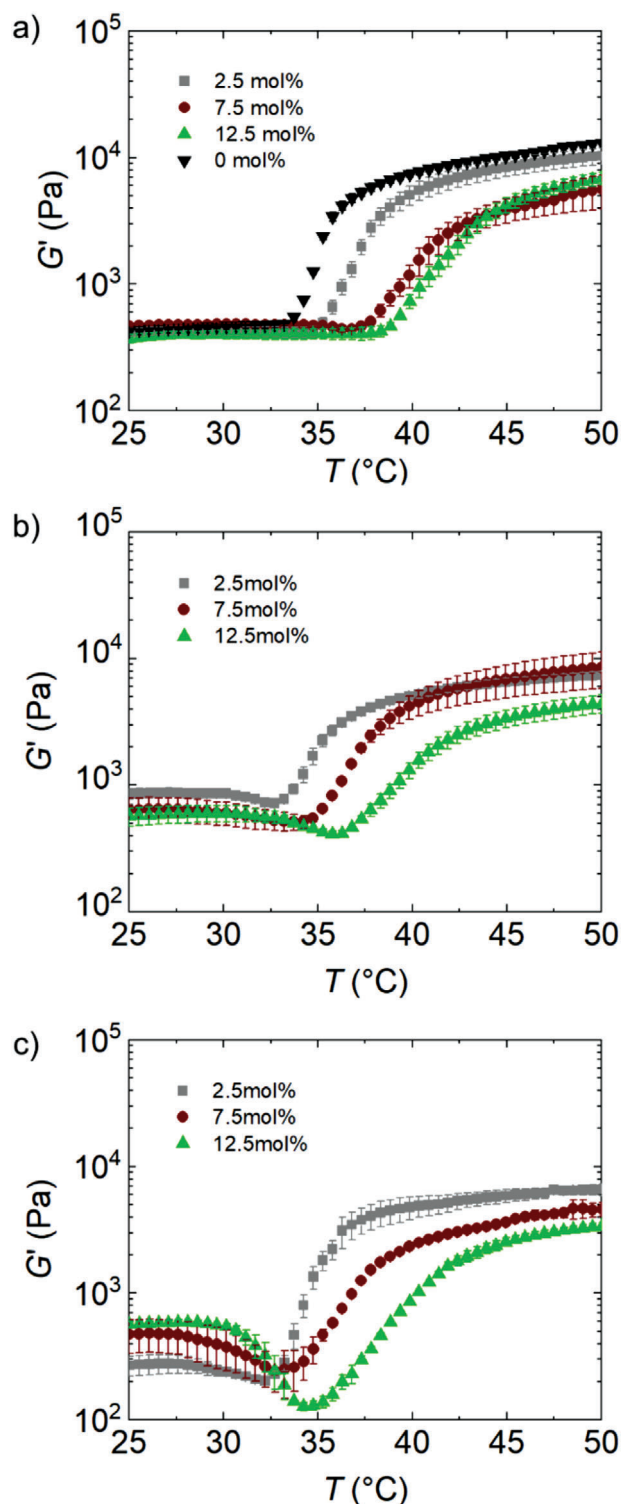


Figure 4. Temperature-dependent rheology measurements of 0 mol% (\blacktriangledown), 2.5 mol% (\blacksquare), 7.5 mol% (\bullet), and 12.5 mol% (\blacktriangle) hydrogels in a) water, b) phosphate buffer, and c) DMEM (10% FBS, 1% Gl., and 1% P/S).

increase at different temperatures. G' (2.5 mol%, \blacksquare) system with the lowest comonomer content increases first with increasing temperature, G' (7.5 mol%, \bullet) system increases later, and G' (12.5 mol%, \blacktriangle) with highest comonomer content increases last. For reference, a G' temperature curve of pure PNIPAAm without any comonomer (0 mol% (\blacktriangledown)) is also shown, with a VPT correspondingly ahead of the other three systems. Figure 4b,c shows rheology measurements of the hydrogels in phosphate buffer and DMEM (10% FBS, 1% Gl., and 1% P/S). Again, G' of the three systems increases with increasing temperature, which is again attributed to the increasing comonomer content within these systems and thus an increasing VPT.

Since the G' versus temperature curves are similar to the swelling curves discussed in the section before, $VPTT_{G'}$ are calculated for the three polymer networks in water, phosphate buffer, and DMEM (10% FBS, 1% Gl., and 1% P/S), and compared to the $VPTT_{SC}$ obtained by the microgel swelling measurements. Respective analysis is shown and discussed in Figure S6 and Table S3 in the Supporting Information, whereby the $VPTT_{G'}$ and $VPTT_{SC}$ values are found to be all in a similar range, which makes the rheology measurements a valuable complement to the swelling measurements described above.

2.1.6. Microgel Properties at Physiological Conditions

So far, we have investigated the temperature-dependent swelling and the mechanical properties of the PNIPAAm/HEAM hydrogels. To further improve their applicability in microtissue engineering, we now focus on the microgel properties at physiological conditions, as assessed by the microgel diameter and mechanical strength in DMEM (10% FBS, 1% Gl., and 1% P/S) at 32 and 37 °C. As reference, also values at 25 °C are considered.

The microgel diameters (d_{norm}) at 25, 32, and 37 °C in DMEM (10% FBS, 1% Gl., and 1% P/S) are obtained in the context of temperature-dependent swelling measurements and represented in a normalized form in Figure 5a, as well as in Table S4 in the Supporting Information, while Figure 5b shows micrographs of single representatives of the different microgel types in DMEM (10% FBS, 1% Gl., and 1% P/S). At 25 °C, all microgel types are in a similar size range, whereas at 37 °C, the microgel diameters increase from 2.5 mol% over 7.5 mol% up to 12.5 mol%, which again can be explained by the increasing comonomer content. The more comonomer is in the polymer network, the more does the VPT shift to higher temperatures, so, microgels with a high comonomer content collapse at higher temperatures than microgels with a low comonomer content, which therefore affects the microgel diameter at given fixed temperature in the range in between. Thus, with increasing comonomer content, the microgels become larger at 37 °C. The mechanical microgel properties are received by temperature-dependent rheology measurements (Figure 4) and represented in Figure 5c, as well as in Table S4 in the Supporting Information. Corresponding values in water and phosphate buffer at 32 and 37 °C are shown in Figure S7 in the Supporting Information. At 25 and 32 °C, the storage modules G' of all three systems are in a similar order of magnitude with values around 200–600 Pa. But even here, an increase in those modules with increasing comonomer content can be observed. In contrast, at 37 °C, values increase up

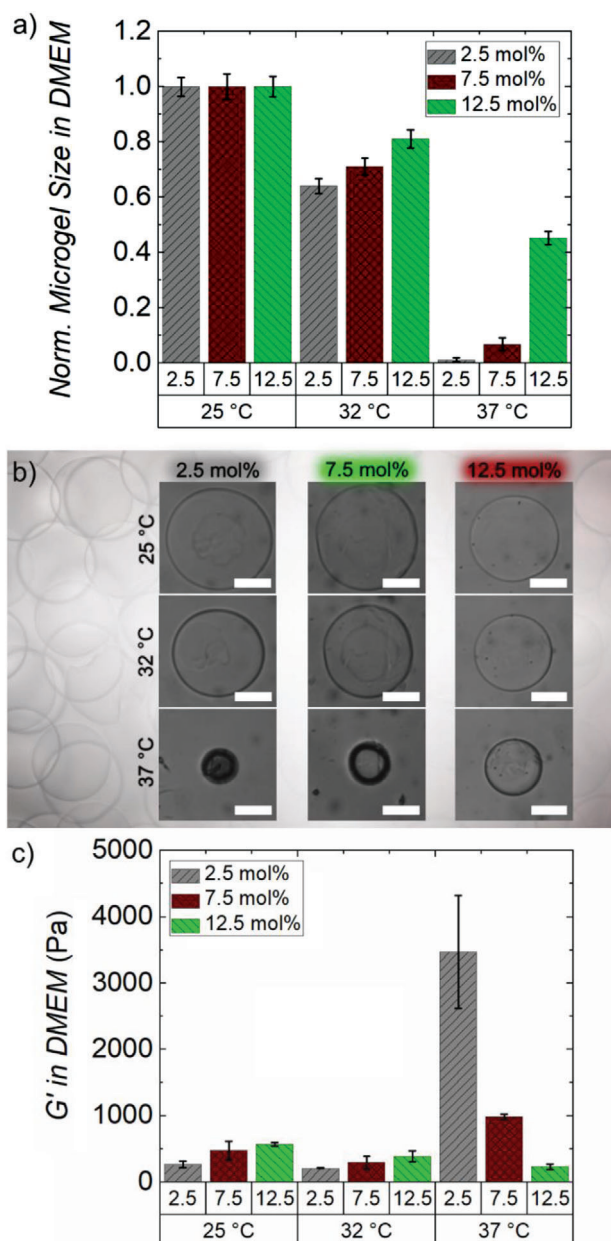


Figure 5. Microgel properties of 2.5, 7.5, and 12.5 mol% PNIPAAm/HEAM polymer networks in DMEM at 25, 32, and 37 °C. a) Normalized microgel diameter. b) Light microscopy imaging of microgels. Scale bars are 50 µm. c) Polymer stiffness.

to (3474 ± 853) Pa for the 2.5 mol% polymer system with less comonomer content, whereas the values decrease with increasing comonomer content up to (231 ± 39) Pa for the 12.5 mol% polymer network. This finding again is explainable by the content of comonomer and the respective differences in the VPT. The more comonomer is in the microgels, the more does the VPT shift to higher temperatures, and so accordingly, the microgels collapse at higher temperatures. Respectively, with increasing comonomer content, microgels become larger, but the amount of polymer in them remains the same, resulting in a lower con-

centration of the remaining polymer backbone contributing to the deformation resistance. For that reason, G' decreases with increasing comonomer content.^[19]

In conclusion, we have analyzed the microgel size of the 2.5, 7.5, and 12.5 mol% systems at 25, 32, and 37 °C, which fit well to the respective G' values. With increasing comonomer content, the microgels become larger, whereas the microgel stiffness decreases. This finding allows us to provide a construction kit of functional microgels with adjustable size and mechanical strength at the physiological relevant temperature range of 32–37 °C.

2.2. Polydopamine Surface Coating

Having tuned and analyzed the thermoresponsive and mechanical properties of 2.5, 7.5, and 12.5 mol% PNIPAAm/HEAM-based polymer networks, we further focus on enhancing their cell-adhesiveness in the following section to make these microgels applicable for cell adhesion and cell growth. To achieve this goal, we focus on the surface modification of the microgels using PDA, as schematically shown in Figure 1-2, since PDA demonstrates cell adhesion-promoting properties and adheres to a multitude of surfaces through physical binding forces.^[20,21]

The strategy of PDA coating is inspired by mussel adhesive proteins, which are largely composed of 3,4-dihydroxy-L-phenylalanine (*L*-DOPA), whose catechol and amino groups are mainly responsible for its strong adhesive properties. Dopamine hydrochloride (DA), the precursor of PDA, contains similar catechol moieties as well as a primary amine function and exhibits analogous adhesive properties in the polymerized state. For this reason, PDA adheres to a variety of surfaces through hydrogen bonding, π - π -stacking and coordination, including PNIPAAm hydrogels.^[21–23] Moreover, DA polymerizes to PDA by autooxidation under mild basic conditions, providing a powerful and simple way to modify PNIPAAm/HEAM microgel surfaces with cell adhesion-promoting properties.

2.2.1. PDA Coating of Macrogels

In a first step, we study the time-dependent PDA coating of PNIPAAm/HEAM hydrogels using the 12.5 mol% gel type. For this purpose, macrogels are synthesized and incubated in a solution of DA in *tris*(hydroxymethyl)aminomethane (TRIS) buffer of pH 8.5 (1 mg mL^{-1}) at room temperature for 0 min (PDA.0), 15 min (PDA.15), 90 min (PDA.90), 3 h (PDA.3h), and 24 h (PDA.24h) as shown in Figure 6a on the right (from the bottom to the top). PDA.0 is colorless and translucent, whereas the black coloration of the hydrogels increases with increasing PDA coating. The black coloration of PDA-coated hydrogels is described in literature and thus a good indication of the successful hydrogel coating.^[24] To further examine that coating, the hydrogels are freeze dried and subsequently analyzed by Fourier-Transform Infrared spectroscopy (FT-IR) using an FT-IR-470 instrument (JASCO Analytical Instruments), along with a reference based on pure PDA (Figure 6a, left). The spectrum of PDA.0 has characteristic signals at 3431 cm^{-1} (O–H and N–H stretching mode), $2840\text{--}3000 \text{ cm}^{-1}$ (C–H stretching modes), and two signals at

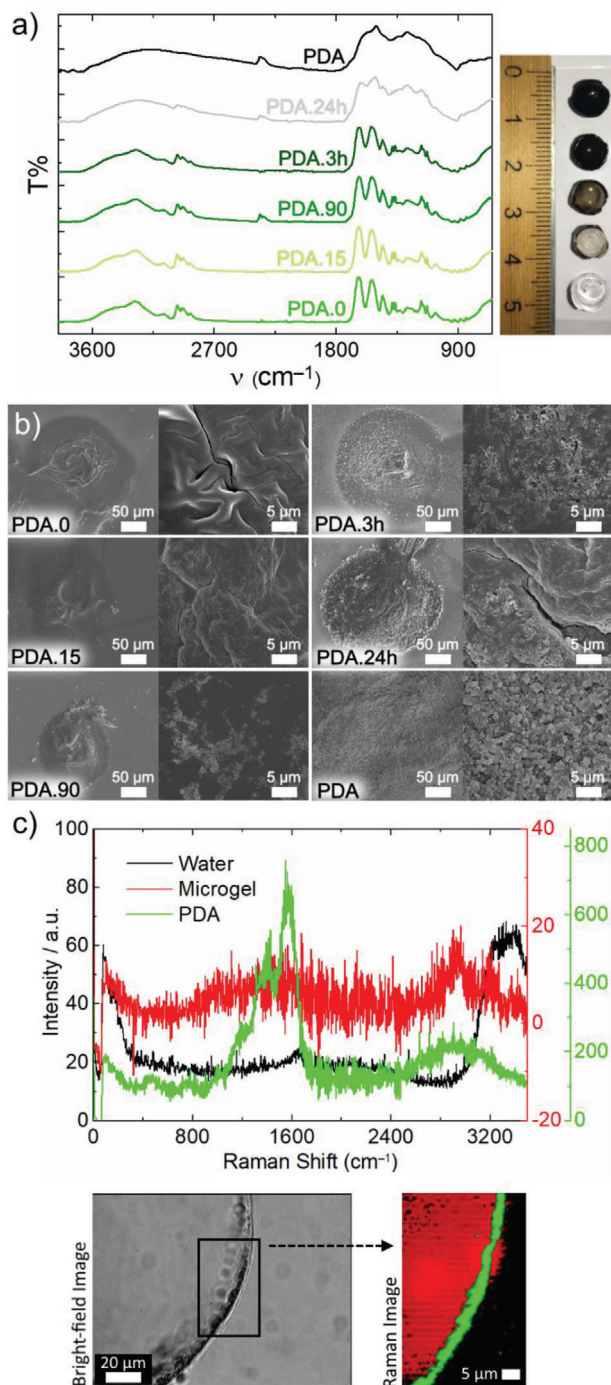


Figure 6. PDA-coated 12.5 mol% PNIPAAm/HEAM hydrogels. a) FT-IR spectroscopy measurements of freeze-dried macrogels and pure PDA (left) and corresponding gels swollen in water (right: from the bottom to the top: PDA.0, PDA.15, PDA.90, PDA.3h, and PDA.24h). b) FE-SEM measurements of freeze-dried microgels and of pure PDA. c) Confocal Raman microscopy measurements of PDA.3h microgels, as well as respective bright-field and Raman images.

1633 cm^{-1} (C=O stretching mode) and 1538 cm^{-1} (N-H bending mode).^[25–27] With increasing PDA coating on the hydrogels, these FT-IR signals are overlaid by characteristic PDA absorbance peaks at 3172 cm^{-1} (phenolic O-H and N-H stretching modes), 1506 cm^{-1} (N-H bending modes), and 1273 cm^{-1} (phenolic C-O stretching modes), also confirming the successful PDA surface coating strategy.^[28,29]

2.2.2. PDA Coating of Microgels

In a second step, the PDA coating procedure is transferred to 12.5 mol% PNIPAAm/HEAM microgels. Corresponding microgels of type PDA.0, PDA.15, PDA.90, PDA.3h, and PDA.24h suspended in isopropanol are shown in Figure S8 in the Supporting Information, where again the increased black coloration confirms PDA surface coating of microgels. Subsequently, the microgels are freeze-dried and morphologically analyzed by field-emission scanning electron microscopy (FE-SEM), as well as pure PDA as a reference. Respective FE-SEM measurements are shown in Figure 6b, whereby the PDA.0 microgels exhibit a plain structure, while pure PDA shows a rough morphology. With increasing PDA coating time, an increase of that rough morphology is observed on the microgels' surfaces. Further FE-SEM images are shown in Figure S9 in the Supporting Information, along with photographs of the freeze-dried PDA.24 microgels (Figure S10, Supporting Information).

To further investigate whether PDA preferentially accumulates on or in the microgels, microgels are analyzed by Confocal Raman microscopy in the swollen state in water. Since the concentration of PDA below 90 min of PDA coating time is not sufficient to record clear Confocal Raman spectra and the fluorescence emitted by PDA leads to highly noisy spectra (Figure S11, Supporting Information), we focus in the following on the PDA.90, PDA.3h, and PDA.24h systems. In Figure 6c, the corresponding spectra for the PDA.3h microgels, as well as the bright-field and Raman images are shown. The PDA spectrum (green) can be clearly distinguished from the water spectrum (black) and the gel spectrum (red). For the PDA, the main bands at 1590 , 1415 , 1350 , and 1240 cm^{-1} and the broadband around 2900 cm^{-1} are detected, the first four peaks correspond to the presence of aromatic rings, while the broadband is attributable to strongly hydrogen-bonded OH and NH stretching vibrations and complies to values in literature.^[30] The resulting spectra indicate enhanced accumulation of PDA on the microgel surface, whereas almost no PDA can be detected inside the microgels. Further analysis also allowed the thickness of the PDA layer on the microgels to be determined (Figure S12, Supporting Information) and revealed a thickness of $\approx 2.3 \pm 0.6\text{ }\mu\text{m}$ for the PDA.90 microgels, $3.1 \pm 1.2\text{ }\mu\text{m}$ for the PDA.3h microgels, and $3.7 \pm 1.8\text{ }\mu\text{m}$ for the PDA.24h microgels.

Whether PDA surface coating of microgels influences temperature-dependent microgel swelling is investigated using PDA.0, PDA.15, PDA.90, PDA.3h, and PDA.24h microgels in phosphate buffer (Figure S13, Supporting Information). All swelling curves show a similar course, indicating almost identical swelling of these microgels. Thus, PDA coating does not seem to have any influence on the microgel swelling, confirming the results of Confocal Raman spectroscopy. With increasing PDA

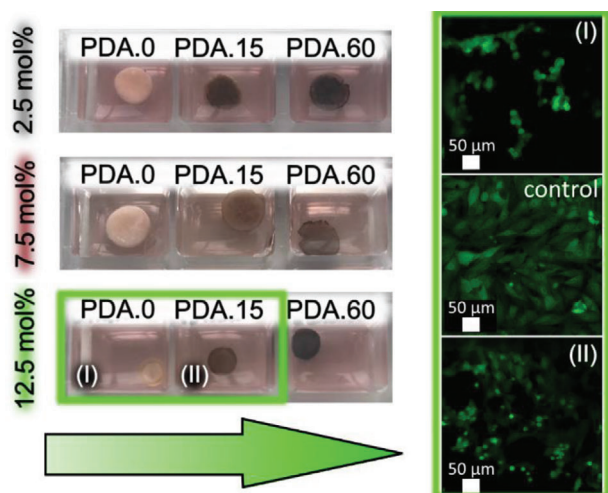


Figure 7. Cell growth on 2.5, 7.5, and 12.5 mol% PNIPAAm/HEAM-PDA hydrogels at 37 °C. Left: Hydrogels with 0, 15, and 60 min of PDA coating, incubated in DMEM (10% FBS, 1% Gl., 1% P/S) at 37 °C and 5% CO₂. Right: CLSM imaging of cells (MG-63-GFP) growing on 12.5 mol% PDA.0 (I) and PDA.15 (II) hydrogels after 24 h incubation time. Both images (I) and (II) are obtained by the 2D fluorescence path of the CLSM. For comparison, a control experiment of cells growing on plastic is also shown.

coating, PDA accumulates on the microgel surface, but hardly any PDA is detectable inside the microgels, thus having little effect on the temperature-dependent microgel swelling.

In summary, we could demonstrate the successful PDA surface modification of 12.5 mol% PNIPAAm/HEAM macro- and microgels. Overall, hence, core-shell microgels are obtained, whereby the microgel cores are less affected from the PDA coating, providing a suitable and functional base for subsequent cell experiments.

2.3. Cell Growth on Microgels

The transfer of PDA-coated PNIPAAm/HEAM microgels to biological applications in microtissue engineering needs to be supported by cellular experiments as schematically shown in Figure 1-3. Hence, we focus in the following on homogenous cell coating of microgels.

2.3.1. Cell Affinity of PDA

To coat core-shell microgels homogeneously with cells, it must be first investigated whether PDA influences cell adhesion on the hydrogels in general. For this reason, we analyze cell growth on 2.5, 7.5, and 12.5 mol% PDA hydrogels with 0 (PDA.0), 15 (PDA.15), and 60 (PDA.60) min of PDA coating. For this purpose, macrogels are synthesized and incubated in a suspension of osteoblasts expressing GFP (MG-63-GFP) and DMEM (10% FBS, 1% Gl., 1% P/S) at 37 °C and 5% CO₂ for several days, whereby cell growth on the hydrogels is analyzed by Confocal Laser Scanning Microscopy (CLSM). Respective images are shown in **Figure 7**. As shown on the left, 2.5 and 7.5 mol% hydrogels precipitate at 37 °C, since their VPTT is far below this temperature.

Hence, they show a whitish, opaque haze and do not shrink in any way. Due to this reason, it is impossible to analyze the cell growth on these hydrogels since transparent materials are required for quantitative CLSM.

In contrast, 12.5 mol% hydrogels show a VPTT in the range of 37 °C, whereby they partly shrink but remain transparent, which makes CLSM possible in these cases. But again, there is a limitation in imaging. Since the intense blackish color of the PDA.60 hydrogels diminishes their transparency, imaging is poorly possible. For this reason, we concentrate on CLSM of the 12.5 mol% PDA.0 and PDA.15 hydrogels. Respective images are shown in Figure 7 on the right, whereby (I) represents the cell adhesion experiments on 12.5 mol% PDA.0 hydrogels, and (II) on 12.5 mol% PDA.15 hydrogels (both: 2D fluorescence path of the CLSM). In (I), large cell clusters are observed, which indicates less cell adhesion on these materials, whereby in (II), the elongated cell morphology argues for excellent cell growth. A control experiment of cells growing on plastic is also shown for comparison.

To extend the hydrogels functionality, we also perform cell experiments at 32 °C as shown in Figure S14 in the Supporting Information. Since the VPTT of all hydrogels are above 32 °C, they are transparent at this temperature and hence suitable for light- and confocal microscopy. Accordingly, we detect cell growth on all three gel types at 32 °C. Thus, the 15 min PDA coating appears to be a valuable approach to enable cell growth on hydrogels, both at 32 and 37 °C. These results provide a stable basis on which to build in subsequent cell experiments on homogenous cell coating of PDA.15 microgels.

2.3.2. Cell Growth on PDA.15 Microgels

To translate the microgel-templates to potential application in microtissue engineering, we need to realize a homogenous cell coating on the microgel surfaces. In general, the PDA coating allows for good cell adhesion, but still there are some factors that complicate a homogenous cell coating to be realized, which is why we need to develop a method to make this possible in general.

One of these factors is the adhesive properties of PDA-coated microgels, which cause microgels to stick onto a multitude of surfaces and other microgels. Corresponding preliminary experiments have been performed and are shown in Figure S15 in the Supporting Information. Since the sticky behavior of PDA-coated microgels is easily circumvented by diluting the microgels in liquid-filled cell culture dishes, this problem can be easily overcome. Another major factor counteracting the homogenous cell coating of microgels in solution is gravity, which is why cells in solution settle on the culture dish bottom over time. If that settling occurs faster than the establishment of cell-gel interactions on the microgel surface, this leads to unoccupied microgel surfaces. Hence, to enable homogenous cell coating of our PDA.15 microgels, we need to address two aspects: i) cell-matrix interactions must be significantly increased, and ii) cells and microgels must be brought into spatial proximity. Taking these factors into account, we investigate in two approaches. First, we focus the nature of the microgel surfaces to promote cell-matrix interactions. Second, we optimize the cell suspension density used in the experiment to bring cells and microgels into spatial proximity.

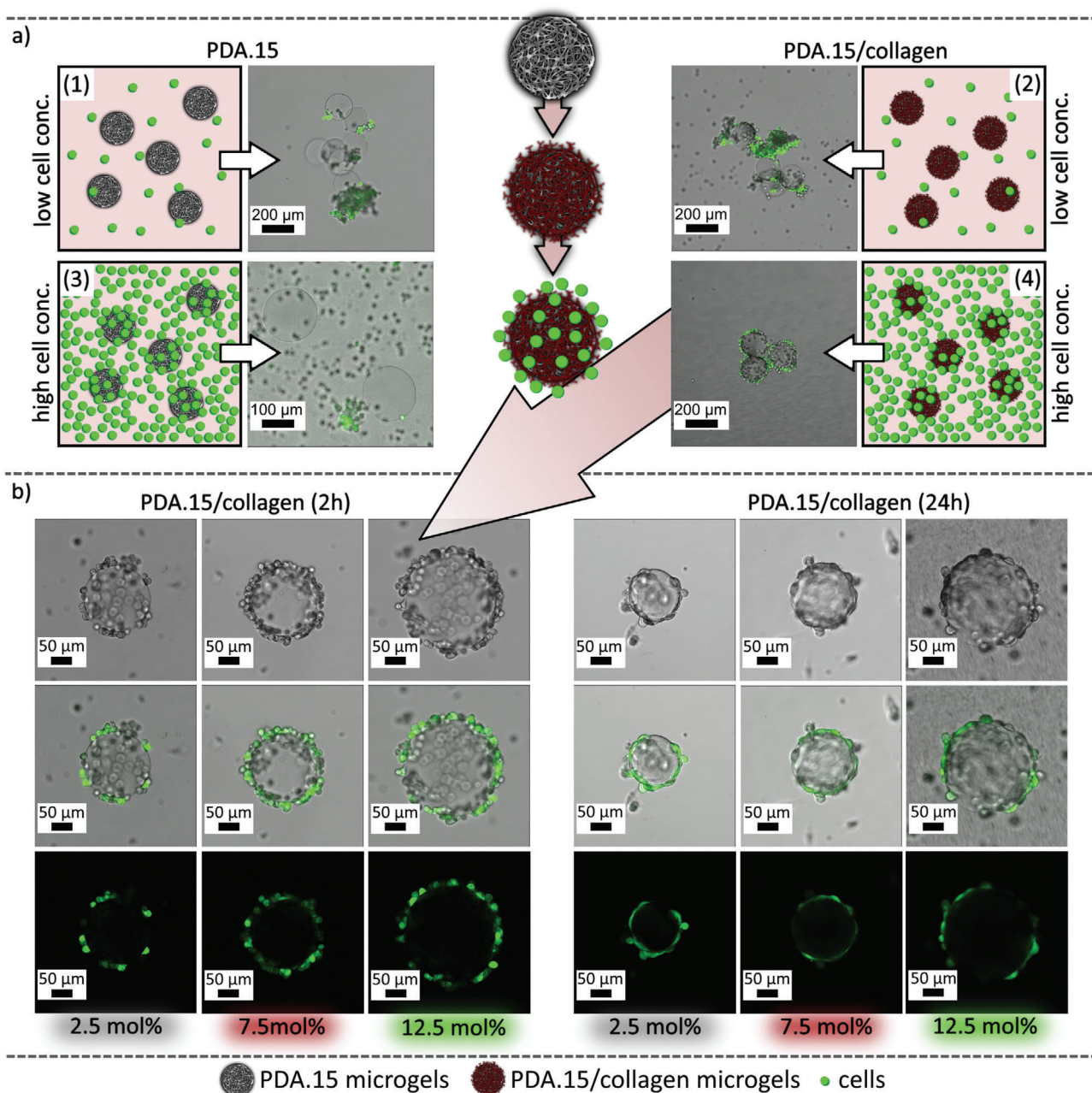


Figure 8. Cell coating of microgels. a) CLSM imaging (superposition of transmission and fluorescence path) of 7.5 mol% PDA.15 and PDA.15/collagen microgels coated with low or high cell concentrations after 24 h incubation time in DMEM (10% FBS, 1% Gl., 1% P/S) at 32 °C and 5% CO₂. b) CLSM imaging (transmission path, fluorescence path, and superposition of both) of cell-coated 2.5, 7.5, and 12.5 mol% PDA.15/collagen microgels after 2 and 24 h incubation time in DMEM (10% FBS, 1% Gl., 1% P/S) at 32 °C and 5% CO₂.

To investigate the influence of different microgel surfaces on cell–matrix interactions, we use two surface types. One type is based on the already characterized PDA.15 microgels, and the second type on PDA.15 microgels with additional collagen coating (PDA.15/collagen microgels). Due to its excellent cell adhesion properties, collagen represents a suitable surface modification substance for microgel coating. Moreover, PDA adheres to a variety of materials, including proteins as collagen,

which essentially facilitates the respective modification of PDA microgel surfaces.^[31]

To examine the effect of different cell concentrations on the homogenous microgel cell coating, PDA.15 and PDA.15/collagen microgels are additionally incubated in two different cell concentrations each (high and low). In summary, we focus on four different cell experiments (1–4), which are schematically shown in Figure 8a. In experiments (1) and (2), PDA.15 and

PDA.15/collagen microgels are incubated at low cell concentrations, respectively. In contrast, in experiments (3) and (4), the PDA.15 and PDA.15/collagen microgels are incubated at high cell concentrations.

In general, cell experiments are performed with osteoblasts expressing GFP (MG-63-GFP), which we trypsinize and detach from the culture dishes at the beginning of each experiment. For the low cell concentration experiments ((1) and (2)), 1.57×10^5 cells mL⁻¹ suspended in DMEM (10% FBS, 1% Gl., 1% P/S) are used. An appropriate volume of cell suspension is transferred to a bioinert Petri dish and mixed with either 7.5 mol% PDA.15 or PDA.15/collagen microgels. The microgels are incubated for 24 h at 32 °C and 5% CO₂ and subsequently analyzed by CLSM, keeping the temperature constant at 32 °C. Respective images are shown in Figure 8a ((1) and (2)). In both approaches, cells are partially adhere to the microgel surfaces and form large cell-microgel clusters, resulting in inhomogenous cell-coated microgel surfaces. In conclusion, both approaches (1) and (2) seem to be unsuitable for homogenous cell coating of microgels.

In contrast, for the high cell concentration experiments ((3) and (4)) 1.57×10^6 cells mL⁻¹ in DMEM (10% FBS, 1% Gl., 1% P/S) are used. The cell suspension is transferred into 96-well plates, and either 7.5 mol% PDA.15 or PDA.15/collagen microgels are added. Leaving the microgels and cells densely packed in the culture dish, the mixture is incubated for 1 h at 32 °C, and 5% CO₂. Subsequently, the microgels are transferred into bio-coated culture dishes containing DMEM (10% FBS, 1% Gl., 1% P/S) to separate them from the remaining free cells. Due to gravity, most of the free cells settle and adhere to the bottom of the bio-coated cell culture plate, so the microgels are easily separable from the remaining cells. Again, the microgels are transferred into new bio-inert culture dish plates and analyzed by CLSM, keeping the temperature constant at 32 °C. In total, PDA.15/collagen microgels are easily coatable with cells by incubating in a highly concentrated cell suspension, while cells do not adhere to the collagen-free PDA.15 microgels. Instead, large cell-microgel agglomerates are observed. This behavior completely contradicts the cell growth on hydrogel surfaces coated with PDA shown in the previous section and is probably caused by the natural binding protein deficit in the highly concentrated cell suspensions, since these proteins are responsible for cell adhesion on PDA coated surfaces. The denser the cell suspension, the less volume of DMEM (10% FBS, 1% Gl., 1% P/S) is present, and thus fewer binding proteins are contained in the FBS. This probably results in an insufficient PDA.15 microgel surface coating with binding proteins from the FBS and prevents cells from adhering well. However, by coating the PDA.15 microgels with collagen beforehand, this problem is avoided. Respective CLSM images are shown in Figure 8a-3 and -4.

Beside 7.5 mol% PDA.15/collagen microgels, also 2.5 and 12.5 mol% microgels are incubated in a highly concentrated cell suspension and subsequently analyzed by CLSM keeping the temperature constant at 32 °C as represented in Figure 8b. The CLSM images on the left show cell-coated microgels after 2 h, and those on the right after 24 h incubation in DMEM (10% FBS, 1% Gl., 1% P/S) at 32 °C and 5% CO₂. The first row demonstrates transmission images, the second superposition of transmission and fluorescence images, and the third fluorescence images of the microgels. After 2 h, cells are homogeneously distributed on

each microgel surface, as shown by their rounded morphology, while after 24 h, their morphology becomes more elongated. This morphology indicates viable cells, adhering and proliferating on the microgel surfaces. To demonstrate the homogeneity of cell coating on the microgels, an image stack is recorded at six levels of a cell-coated 12.5 mol% PDA.15/collagen microgel, as shown in Figure S16 in the Supporting Information.

As all three microgel systems are incubated in DMEM (10% FBS, 1% Gl., 1% P/S) at 32 °C and 5% CO₂, significant differences in the microgel size are recognizable. Overall, an increase in diameter is observed within the 2.5 mol% through 7.5 mol% up to 12.5 mol% systems, which can be attributed to the increasing comonomer content. The more comonomer, the more does the VPT shift toward higher temperatures, and the larger the microgels become. This additionally affects the mechanical strength of the microgels, which decreases within the three systems as discussed above. However, since the cells adhere evenly distributed on all three microgel systems, no effects of the respective microgel properties on cell growth are observed.

In total, we could demonstrate the ability to obtain a homogenous cell coating of core-shell microgels by increasing cell-matrix interactions using collagen and a high concentrated cell-suspension. Additionally, a microgel-type independent cell adhesion is observed, meaning cells are unaffected from the 2.5, 7.5, and 12.5 mol% microgel size and mechanical strength. This finding enables a system-independent and thus universal use of the microgel templates in potential follow-up studies for microtissue engineering applications, such as mimicking the blastula in embryogenesis, breast glands, and the alveolar epithelium.^[32–34]

2.3.3. Microgels Incorporated in Cell Spheroids

Since spheroids are commonly used 3D cell culture models for microtissue engineering and drug screening applications, we investigate the mimicking of higher hierarchical spheroid structures with tunable mechanical properties using our core-shell microgel platform. Toward this end, 7.5 mol% PDA.15 microgels are coated with fibronectin to improve their cell adhesions properties. Subsequently, they are added to MCF7 cells and seeded into cell spheroid cultures. After 24 h, microgel-laden cell spheroids are formed at 30 °C with one to three integrated microgels (Figure 9), whereby the number of integrated microgels depends on the number of microgels added to each well. The thermoresponsive microgel properties allowed altering the microgel size and analyzing the stability of microgel-laden spheroid structures. When the temperature is increased from 30 to 37 °C, the microgels within the spheroids shrink and the cells follow the movement induced by the microgels. Next, when the temperature is decreased again to 30 °C, the spheroids recover their initial structure and the microgel swell to their initial volume. The shrinking of the microgels is fast within a few seconds, yet the reaction of the cells is slower and takes place within 20 min, as shown in Movie S1 in the Supporting Information. This behavior is explainable by the strong cell-cell adhesion and high E-cadherin expression of MCF7 cells, which presumably leads to the stability of the multicellular structure during this movement. In summary, this finding offers a temperature-sensitive cell spheroid platform with tunable

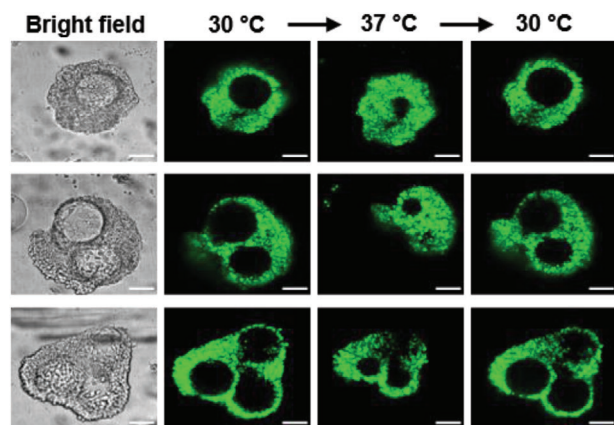


Figure 9. Fibronectin-coated 7.5 mol% PDA.15 microgels incorporated in cell spheroid structures based on MCF7 cells. On the left, bright field micrographs of spheroids at 30 °C are shown, and on the right, confocal fluorescence micrographs are added. The MCF7 cells are stained with vibrant DiO (green fluorescence). The temperature is first increased from 30 to 37 °C and later decreased back to 30 °C. Scale bars are 100 µm.

mechanical properties as basis for future investigations on higher hierarchical spheroid structures.

3. Conclusion

Since 3D in vitro microtissue models offer a suitable approach to reduce and replace animal testing, we have developed microtissue systems using a core-shell micro-template platform that takes into account the complex shape, the nature, and the mechanical properties of in vivo tissues to best mimic the in vivo environment. These microgels were synthesized and analyzed with a primary focus on material design such to obtain a deep understanding at the conceptual level through 1) systematic tuning of the mechanical and functional properties of the microgel cores, 2) enhancement of their cell adhesiveness, and 3) application in cell biology.

In the first development step, by using microfluidic technology, we were able to obtain spherical cores whose mechanical properties could be tuned by choosing a thermoresponsive polymer and different proportions of hydrophilic comonomers, essentially simplifying the mimicking of natural microstructures. In the second step, we were able to increase the attractiveness of the microgel cores to cell adhesion by effective PDA surface coating, while minimizing its influence on the mechanical and functional properties of the cores. In the last step, we demonstrated the successful homogenous cell coating of the core-shell microgels, using additional collagen surface coating, and also presented the successful embedment of fibronectin-coated microgels into cell spheroid structures and their response to temperature changes.

Thus, the present core-shell microcarrier toolkit enables a multifunctional and versatile 3D microtissue platform and can be used as flexibly adjustable template for the in vitro formation and analysis of hollow spherical tissue constructs, as well as for the investigations on higher hierarchical spheroid structures.

4. Experimental Section

Materials: NIPAAm and APS were purchased from Acros Organics. HEAM, TEMED, SPAN 80, dopamine hydrochloride, trypsin EDTA solution, phosphate buffer (DPBS-D8537), DMEM high glucose (D5796), fetal bovine serum (FBS) (F7524), Penicillin-Streptomycin (P/S) (P4333), and tris(hydroxymethyl)aminomethane were obtained from Sigma-Aldrich. BIS was obtained from Merck, Novec 7500 from 3M, Krytox 157FS(L) from DuPont, 1H,1H,2H,2H-perfluoro-1-octanol from Alfa-Aesar and gibco GlutaMAX (GL), as well as gibco collagen I (Rat Tail) from Thermo Fisher Scientific. Deuterium oxide was purchased from deuterio. Osteoblasts (MG-63-GFP) were obtained from R. E. Unger (Johannes Gutenberg-University Mainz, Institute of Pathology).

Hydrogel Synthesis: NIPAAm was recrystallized twice from *n*-hexane before use in hydrogel synthesis. 0, 2.5, 7.5, and 12.5 mol% hydrogels were synthesized by mixing NIPAAm (0 mol%: 99.0 mg, 0.875 mmol, 0.990 eq.; 2.5 mol%: 96.5 mg, 0.853 mmol, 0.965 eq.; 7.5 mol%: 91.5 mg, 0.809 mmol, 0.915 eq.; 12.5 mol%: 86.5 mg, 0.764 mmol, 0.865 eq.), HEAM (0 mol%: 0.0 mg, 0.000 mmol, 0.000 eq.; 2.5 mol%: 2.5 mg, 0.021 mmol, 0.025 eq.; 7.5 mol%: 7.0 mg, 0.061 mmol, 0.075 eq.; 12.5 mol%: 11.0 mg, 0.096 mmol, 0.125 eq.), BIS (1.3 mg, 0.009 mmol, 0.010 eq.), APS (4.9 mg, 0.021 mmol, 0.025 eq.), and water (1 mL). Subsequently, the aqueous solution was transferred into a 96-well plate (70 µL per well). Gelation was initiated by adding TEMED (1 µL per well). After 10 min, gelation occurred, and gels were purified by incubation in water over 3 days while changing the water twice per day.

Microgel Synthesis: Droplet-based microfluidics was carried out using a PDMS device fabricated by soft lithography as described in Figure S2 in the Supporting Information. The PDMS device was connected to two syringe pumps (neMESYS Plugin) via polyethylene tubing (Intramedic Clay Adams Brand PE20) and plastic syringes (Becton Dickinson). NIPAAm was recrystallized twice from *n*-hexane before use in the microgel synthesis. For the synthesis of 2.5, 7.5, and 12.5 mol% microgels, NIPAAm (2.5 mol%: 96.5 mg, 0.853 mmol, 0.965 eq.; 7.5 mol%: 91.5 mg, 0.809 mmol, 0.915 eq.; 12.5 mol%: 86.5 mg, 0.764 mmol, 0.865 eq.), HEAM (2.5 mol%: 2.5 mg, 0.021 mmol, 0.025 eq.; 7.5 mol%: 7.0 mg, 0.061 mmol, 0.075 eq.; 12.5 mol%: 11.0 mg, 0.096 mmol, 0.125 eq.), BIS (1.3 mg, 0.009 mmol, 0.010 eq.), and APS (4.9 mg, 0.021 mmol, 0.025 eq.) are dissolved in water (1 mL) and injected with a flow rate of 450 µm h⁻¹ into the PDMS device. At the cross-junction of the microchannel, the aqueous solution was broken to form monodisperse pre-microgel droplets by flow-focusing with an immiscible oil (Novec 7500), which was injected with a flow rate of 1500 µm h⁻¹. To stabilize the resulting droplets, 2 wt% of Krytox and 3 wt% TEMED were added to the fluorinated oil. Resulting droplets were purified after 24 h gelation time with Novec 7500 containing 20 wt% 1H,1H,2H,2H-perfluoro-1-octanol (3 × 400 µL), pure Novec 7500 (3 × 400 µL), *n*-hexane containing SPAN 80 surfactant (1 wt%) (3 × 400 µL), pure *n*-hexane (3 × 400 µL), 2-propanol (3 × 400 µL), and 1,4-dioxane (3 × 400 µL). The microgels were cooled to 5 °C and washed with cold water. Depending on the application, the microgels were transferred to phosphate buffer (DPBS-D8537) or DMEM (10% FBS, 1% GL, 1% P/S).

Microgel Swelling: Swelling measurements were carried out using microgels of type 2.5, 7.5, and 12.5 mol% synthesized via microfluidics as described above. Samples were incubated in water, phosphate buffer (DPBS-D8537), and DMEM (10% FBS, 1% GL, and 1% P/S) placed on a thermoelectric stage from Instec, while heating up from 25 to 50 °C in 1 °C 10 min⁻¹ steps. After equilibration for 10 min, an optical micrograph was taken at each temperature step with a high-resolution digital camera from Carl Zeiss. The pictures were analyzed, and particle sizes were determined using the ImageJ software.

Rheology: For elasticity measurements of the 0, 2.5, 7.5, and 12.5 mol% systems, hydrogels of 300 µL volume were synthesized using a rounded cap of 1.8 cm diameter for shaping, while the hydrogel compositions referred to that described above. After 10 min of gelation, gels are purified by incubation in water over 3 days while changing the water twice per day. Subsequently, hydrogels were transferred into phosphate buffer (DPBS-D8537) or DMEM (10% FBS, 1% GL, 1% P/S) and applied to rheology after incubation time of 24 h in the respective solvent. Rheological

measurements were performed using an Anton Paar modular compact rheometer of type MCR 302 (Anton Paar, Graz, Austria) equipped with a plate–plate measuring system PP25 (2.5 cm diameter) and solvent trap. Temperature-dependent elasticity measurements were carried out a constant shear amplitude of 1% and a constant shearing frequency of 1 rad s^{-1} each as well as using a constant normal force of $F_N = 1 \text{ N}$. Measuring points were recorded while the rheometer heated up from 25 to 50 °C in 1 °C min^{-1} steps. Measurements in the linear-viscoelastic (LVE) regime were confirmed by amplitude sweeps, whereby the frequency remained constant at 1 rad s^{-1} and the amplitude was varied between 0.01% and 100% deformation. In addition, frequency sweeps were performed in a frequency range between 100 and 0.01 rad s^{-1} and at a fixed amplitude of 1% within the LVE regime of the sample.

PDA Coating: 12.5 mol% hydrogels and microgels were synthesized as described above and incubated in a 1 mg mL^{-1} solution of dopamine hydrochloride (DA) and *tris*(hydroxymethyl)aminomethane (TRIS) buffer of pH 8.5 on a shaking plate at room temperature. PDA.0 hydrogels were incubated for 0 min, PDA.15 hydrogels for 15 min, PDA.90 hydrogels for 90 min, PDA.3h for 3 h, and PDA.24h for 24 h. After coating, hydrogels were purified by incubation in water over 24 h by changing water five times. Microgels were purified by washing with water five times and using a centrifuge (10 000 rpm, 5 min, 5 °C). Pure PDA as reference was synthesized by incubating 1 mg mL^{-1} dopamine hydrochloride (DA) in a TRIS buffer solution (pH 8.5) for 24 h at room temperature. 10% acetone was added, and PDA was separated from the PDA/TRIS buffer solution by centrifugation (10 000 rpm, 20 min, 5 °C). The black powder was purified by washing with water five times and using a centrifuge (10 000 rpm, 5 min, 5 °C).

FE-SEM: FE-SEM measurements were performed on a NOVA Nano-SEM 630 with an attached Oxford Inca X-ray system for chemical analysis. Freeze-dried samples were sputtered with a gold-layer of 10 nm before analysis. Secondary and backscattered electron images were collected with an acceleration voltage of 10 keV and a spot size of 5 using a through-the-lens detector.

MAS NMR Spectroscopy: All NMR experiments were performed on a Bruker Avance DSX 400 NMR spectrometer operating at $399.87 \text{ MHz } ^1\text{H}$ frequency. Prior to the ^1H NMR experiments, all gels were incubated in D_2O for 24 h at room temperature, while solvent was changed three times. The gel samples were measured using 4 mm rotors and inserts specially developed to investigate gels and soft matter. The ^1H single pulse excitation NMR spectra were recorded using a commercial three channel Bruker 4 mm probe head at 3 kHz magic angle spinning (MAS), averaging 32 scans with a 20 s recycle delay.

Confocal Raman Spectroscopy: Confocal Raman spectroscopy was performed with a Witec 300 alpha R setup. During the measurement, 12.5 mol% PDA-coated microgels were illuminated with a 532 and 633 nm excitation line from a single mode frequency doubled Nd:YAG laser via a $100 \text{ }\mu\text{m}$ single-mode glass fiber. Emitted light was focused on a Zeiss C-Apochromat 63x/1.2 W objective, while the laser power at the sample behind the objective was 0.5 mW to avoid damage of the sample. To further separate the Raman signals from the excitation line, an edge filter was installed. The confocal character of the Raman signal was achieved via a $50 \text{ }\mu\text{m}$ multi-mode fiber glass between microscope and the Raman spectrometer, where the fiber served as a pinhole. The Raman spectrometer was equipped with a holographic grating of 600 lines per mm. As detector, a Newton Andor EMCCD camera with 1600×200 pixels was used. With this configuration, a spectral resolution of about 2 cm^{-1} was obtained and a spatial resolution of 270 nm (lateral). All data sets were analyzed using cluster analysis and nonnegative matrix factorization. The cross-sections calculation was obtained from the average of a 10 mm thick line perpendicular to the PDA layer.

Cell Coating of Microgels: Osteoblasts (MG-63-GFP) cultivated in Petri dishes with an area of 11.9 cm^2 and of 80% confluency were detached from plastic by trypsinization using trypsin EDTA solution. After centrifugation (1000 rpm, 5 min), the resulting cell pellet was resuspended in DMEM (10% FBS, 1% Gl., 1% P/S) and adjusted to a specific cell concentration, while cell counting was performed using a Neubauer counting chamber. Depending on the cell experiment, different amounts of cells were used as described in the following. For the cell growth on macrogels, 2.5, 7.5,

and 12.5 mol% hydrogels of type PDA.0, PDA.15, and PDA.60 were synthesized as described above and incubated in phosphate buffer (DPBS-D8537). Subsequently hydrogels were transferred into 8-well plates from ibidi and covered with 300 μL of cell suspension in DMEM (10% FBS, 1% Gl., 1% P/S) at a final concentration of $1.57 \times 10^5 \text{ cells mL}^{-1}$ each. The cell-coated hydrogels were incubated at 37 °C and 5% CO_2 , as well as at 32 °C and 5% CO_2 for several days and analyzed by optical microscopy (Zeiss Axio) and CLSM. For cell growth on microgels, 2.5, 7.5, and 12.5 mol% PDA.15 microgels were synthesized as described above and transferred in phosphate buffer (DPBS-D8537). Additionally, 2.5, 7.5, and 12.5 mol% PDA.15/collagen microgels were synthesized, by incubating PDA.15 microgels in a solution of $50 \text{ }\mu\text{g mL}^{-1}$ collagen in $20 \times 10^{-3} \text{ M}$ acetic acid at room temperature for 1 h. Afterward, microgels were purified by washing three times with phosphate buffer (DPBS-D8537) using a centrifuge (10 000 rpm, 5 min, 5 °C). For the low cell concentration experiments (1) and (2), $1.57 \times 10^5 \text{ cells mL}^{-1}$ suspended in 3 mL DMEM (10% FBS, 1% Gl., 1% P/S) were transferred to a bioinert Petri dish and mixed with 10–20 7.5 mol% PDA.15 or PDA.15/collagen microgels and incubated for 24 h at 32 °C and 5% CO_2 . For the high cell concentration experiments (3) and (4), $1.57 \times 10^6 \text{ cells mL}^{-1}$ suspended in 300 μL DMEM (10% FBS, 1% Gl., 1% P/S) were transferred into a 96-well plate and 5–10 7.5 mol% PDA.15 or PDA.15/collagen microgels were added. The mixture was incubated for 1 h at 32 °C and 5% CO_2 and subsequently transferred into a bio-coated culture dish containing DMEM (10% FBS, 1% Gl., 1% P/S). Again, microgels were incubated for 1 h at 32 °C and 5% CO_2 and subsequently transferred to a bio-inert culture dish plate and analyzed by CLSM, keeping the temperature constant at 32 °C. CLSM analysis was performed using a Leica TCS-SP8 AOBs SMD microscope with an HCPL APO CS2 $10 \times /0.40$ DRY objective. Cells expressing GFP were excited with an argon laser (488 nm), while fluorescence was detected between 500 and 600 nm using a PMT2 detector. Transmission was detected using a PMT Trans detector.

Spheroid Culture: The MCF7 human breast cancer cells (ATCC Cat. No. HTB-22) were cultured in DMEM (Gibco, 10565018), supplemented with 10% FBS (Sigma Aldrich, F2442), and 1% PS (Jena Bioscience, ML-105XL) at 37 °C and 5% CO_2 using standard cell culture methods. The 7.5 mol% PDA.15 microgels were incubated with 10–20 $\mu\text{g mL}^{-1}$ human plasma fibronectin (Millipore Cat. # FC010) for 1 h at room temperature with mild agitation. The microgels were washed twice with PBS buffer and used immediately in cell culture. Cells were grown to 80% confluence and the cells were stained with the vibrant Dio cell-labeling solution (Thermo Fisher Cat. No. V22886) following the manufacture's protocol. The cells were detached with trypsin from the flask and resuspended in spheroid media (DMEM containing 3% FBS, 1% PS, and 0.6% methylcellulose (Sigma Aldrich Cat. # M7027)). The cells were counted using a cell counter (BioRad, TC20) and diluted to $2 \times 10^3 \text{ cells mL}^{-1}$. The microgels were added to the cell suspension in a 1–3 microgels per 200 cells. 100 μL of the cell-microgel mixture (200 cells, 1–3 microgels) per well was pipetted into a U-bottom 96 well plate (Greiner bio-one Cat. # 650 185). The plate was centrifuged at 200 rcf for 3 min and cultured at 30 °C for 24 h. Total internal reflections and fluorescence images (488 nm excitation laser) confocal microscopy (Leica SP8) equipped with a temperature controller. Images were acquired initially at 30 °C, then the temperature was increased to 37 °C and subsequently again at 30 °C.

Supporting Information

Supporting Information is available from the Wiley Online Library or from the author.

Acknowledgements

Parts of the results of this study were acquired with a confocal laser scanning microscope funded in part by the Major Research Instrumentation Program of the German Research Foundation under grant no. INST 247/878-1 FUGG. The authors wish to thank Ronald E. Unger (JGU Mainz,

Institute for Pathology) for providing osteoblasts expressing GFP (MG-63-GFP). Further thanks go to Alena Kuzmina for practical support and to Simone Stengelin for photography. S.V.W. thanks the European Research Council for the ERC Starting Grant ARTIST (# 757593). The author name "Seraphine V. Wegner" was corrected on September 15, 2021.

Open access funding enabled and organized by Projekt DEAL.

Conflict of Interest

The authors declare no conflict of interest.

Data Availability Statement

The data that support the findings of this study are available from the corresponding author upon reasonable request.

Keywords

3R principle, microfluidics, microgels, microtissue engineering, stimuli-responsive polymers, polydopamine surface coating

Received: May 17, 2021

Revised: July 9, 2021

Published online: August 3, 2021

- [1] P. Bédard, S. Gauvin, K. Ferland, C. Caneparo, È. Pellerin, S. Chabaud, S. Bolduc, *Bioengineering* **2020**, 7, 115.
- [2] F. Fontana, M. Raimondi, M. Marzagalli, M. Sommariva, N. Gagliano, P. Limonta, *Int. J. Mol. Sci.* **2020**, 21, 6806.
- [3] R. Edmondson, J. J. Broglie, A. F. Adcock, L. Yang, *Assay Drug Dev. Technol.* **2014**, 12, 207.
- [4] E. Stengelin, A. Kuzmina, G. L. Beltramo, M. F. Koziol, L. Besch, R. Schröder, R. E. Unger, W. Tremel, S. Seiffert, *Adv. Healthcare Mater.* **2020**, 6, e1901820.
- [5] T. Rossow, P. S. Lienemann, D. J. Mooney, *Macromol. Chem. Phys.* **2017**, 218, 1600380.
- [6] J. Feng, J. Dou, Y. Zhang, Z. Wu, D. Yin, W. Wu, *Polymers* **2020**, 12, 547.
- [7] R. Begum, Z. H. Farooqi, E. Ahmed, A. Sharif, W. Wu, A. Irfan, *RSC Adv.* **2019**, 9, 13838.
- [8] L. Yang, X. Fan, J. Zhang, J. Ju, *Polymers* **2020**, 12, 389.
- [9] H. L. Judah, P. Liu, A. Zarbakhsh, M. Resmini, *Polymers* **2020**, 12, E2590.
- [10] S. Seiffert, *Macromol. Rapid. Commun.* **2011**, 32, 1600.
- [11] K. Nagase, M. Yamato, H. Kanazawa, T. Okano, *Biomaterials* **2018**, 153, 27.
- [12] N. Kaushik, L. Nhat Nguyen, J. H. Kim, E. H. Choi, N. Kumar Kaushik, *Int. J. Mol. Sci.* **2020**, 21, 6544.
- [13] J. H. Ryu, P. B. Messersmith, H. Lee, *ACS Appl. Mater. Interfaces* **2018**, 10, 7523.
- [14] H. Lee, S. M. Dellatore, W. M. Miller, P. B. Messersmith, *Science* **2007**, 318, 426.
- [15] L. Zhang, Z. Liu, L.-Y. Liu, J.-L. Pan, F. Luo, C. Yang, R. Xie, X.-J. Ju, W. Wang, L.-Y. Chu, *ACS Appl. Mater. Interfaces* **2018**, 10, 44092.
- [16] M. Seuss, W. Schmolke, A. Drechsler, A. Fery, S. Seiffert, *ACS Appl. Mater. Interfaces* **2016**, 8, 16317.
- [17] G. Fundueanu, M. Constantin, I. Asmarandei, S. Bucatariu, V. Harabagiu, P. Ascenzi, B. C. Simionescu, *Eur. J. Pharm. Biopharm.* **2013**, 85, 614.
- [18] J. E. S. Sayed, C. Lorthioir, P. Perrin, N. Sanson, *Soft Matter* **2019**, 15, 963.
- [19] N. Adrus, M. Ulbricht, *React. Funct. Polym.* **2013**, 73, 141.
- [20] J. Lin, W. Wang, J. Cheng, Z. Cui, J. Si, Q. Wang, W. Chen, *J. Appl. Polym. Sci.* **2020**, 137, 49252.
- [21] H. A. Lee, E. Park, H. Lee, *Adv. Mater.* **2020**, 32, e1907505.
- [22] J. Saiz-Poseu, J. Mancebo-Aracil, F. Nador, F. Busqué, D. Ruiz-Molina, *Angew. Chem., Int. Ed.* **2019**, 58, 696.
- [23] C.-T. Kao, C.-C. Lin, Y.-W. Chen, C.-H. Yeh, H.-Y. Fang, M.-Y. Shie, *Mater. Sci. Eng., C* **2015**, 56, 165.
- [24] Y. Wu, C. Yu, M. Xing, L. Wang, G. Guan, *J. Biomed. Mater. Res., Part B* **2020**, 108, 117.
- [25] X. Zhang, W. Shen, J. Dou, Y. Meng, S. Fang, R. Liu, *J. Appl. Polym. Sci.* **2020**, 137, 48486.
- [26] M. H. Futscher, M. Philipp, P. Müller-Buschbaum, A. Schulte, *Sci. Rep.* **2017**, 7, 17012.
- [27] X. Xu, B. Bai, H. Wang, Y. Suo, *ACS Appl. Mater. Interfaces* **2017**, 9, 6424.
- [28] F. Xu, S. Xie, R. Cao, Y. Feng, C. Ren, L. Wang, *Sens. Actuator, B* **2017**, 243, 609.
- [29] X. Liu, J. Cao, H. Li, J. Li, Q. Jin, K. Ren, J. Ji, *ACS Nano* **2013**, 7, 9384.
- [30] M. L. Alfieri, R. Micillo, L. Panzella, O. Crescenzi, S. L. Oscurato, P. Maddalena, A. Napolitano, V. Ball, M. d'Ischia, *ACS Appl. Mater. Interfaces* **2018**, 10, 7670.
- [31] J.-L. Wang, K.-F. Ren, H. Chang, F. Jia, B.-C. Li, Y. Ji, J. Ji, *Macromol. Biosci.* **2013**, 13, 483.
- [32] C. Spiteri, V. Caprettini, C. Chiappini, *Biomater. Sci.* **2020**, 8, 6992.
- [33] A. Gaiko-Shcherbak, G. Fabris, G. Dreissen, R. Merkel, B. Hoffmann, E. Noetzel, *PLoS One* **2015**, 10, e0145174.
- [34] K. J. R. Lewis, M. W. Tibbitt, Y. Zhao, K. Branchfield, X. Sun, V. Balasubramaniam, K. S. Anseth, *Biomater. Sci.* **2015**, 3, 821.